We are IntechOpen, the world's leading publisher of Open Access books Built by scientists, for scientists

4,800
Open access books available

122,000
International authors and editors

135M
Downloads

Our authors are among the

154
Countries delivered to

TOP 1%
most cited scientists

12.2%
Contributors from top 500 universities

CLARIVATE ANALYTICS BOOK CITATION INDEX INDEXED

WEB OF SCIENCE™

Selection of our books indexed in the Book Citation Index in Web of Science™ Core Collection (BKCI)

Interested in publishing with us?
Contact book.department@intechopen.com

Numbers displayed above are based on latest data collected.
For more information visit www.intechopen.com

12

Model-based Data Fusion in Industrial Process Instrumentation

Gerald Steiner
Institute of Electrical Measurement and Measurement Signal Processing
Graz University of Technology
Austria

1. Introduction

Process sensors form an essential component of modern industrial production processes. They usually have to be operated under stringent environmental, safety, and cost constraints. Some of the key requirements on process instrumentation are: operation under harsh and varying environmental conditions, high reliability, fault tolerance, and low cost. The failure of process sensors may cause high losses due to plant breakdowns or out-of-specification products. Therefore it is important to know as much as possible about the momentary states of a production process. In addition, the estimates need to have low uncertainty and high reliability.

Sensor and data fusion can be key techniques to economically reach these goals and achieve higher performance than with isolated single point sensors alone. These methods enable the quantification of otherwise inaccessible quantities that cannot be deduced from a single sensor or management principle. Examples are the concentration measurement of ternary solutions or the tomographic estimation of spatially distributed material parameters from arrays of single point sensors. Industrial processes are usually operated within a defined environment, although there may be very harsh conditions like temperature variations, aggressive fluids, and high humidity. There are certain limits of operation. The nominal parameters, like desired product specifications as well as normal or acceptable fluctuations are known in advance while unknown encounters like in classical sensor fusion for target tracking, autonomous guidance, and battlefield surveillance are not within the scope of operation.

This fact potentially establishes a precise and specific model of the industrial process at hand. The knowledge then contained in the process model can be fruitfully exploited in model-based data fusion. Generally, model-based approaches reach beyond straightforward methods like physical redundancy with majority votings or heuristic filtering operations. The achievable measurement precision as well as decision making reliability is usually higher in model-based approaches due to the additional regularization of the state or hypotheses space that is achieved with an appropriate model. However, at the same time special care needs to be taken to choose a model that allows for sufficient and representative variation. This is the only way the inherent variability of a process can be adequately represented.

Source: Sensor and Data Fusion, Book edited by: Dr. ir. Nada Milisavljević,
ISBN 978-3-902613-52-3, pp. 490, February 2009, I-Tech, Vienna, Austria

The well-known JDL (Joint Directors of Laboratories) data fusion process model is a popular and useful conceptual framework for the classification and comparison of data fusion approaches (Hall & Llinas, 1997), (Varshney, 1997), (Macii et al., 2008). It was originally developed with military applications like surveillance and target tracking in mind. It has been pointed out that the JDL model does not fully address data fusion problems from non-military areas, like image fusion. However, a classification of such fusion algorithms may be useful for a common understanding. After a preprocessing stage the JDL model distinguishes four levels of processing:

- Object refinement (level 1)
- Situation refinement (level 2)
- Threat refinement (level 3)
- Process refinement (level 4)

Due to the frequent availability of a well-defined process description, the model-based data fusion approaches in industrial process instrumentation are classified as level 1 processes in most cases. In this object refinement stage parametric, locational, and identity information are combined. Major functions are the transformation and alignment of data to a suitable reference frame, and the estimation and prediction of states. In terms of process instrumentation, the desired output of the object refinement process are quantitative and unambiguous figures. Due to the precise knowledge of the desired target quantities these figures can be straightforwardly used for an objective assessment of the industrial process. Therefore the higher levels of the JDL model do not play an as important role in industrial as in military applications.

According to another popular characterization of data fusion approaches the fusion can take place at different stages of the signal processing chain. A common categorization uses three levels (Varshney, 1997), (Hall et al., 1999):

- Data-level fusion
- Feature-level fusion
- Decision-level fusion

In data-level fusion the raw data from each of the sensors are combined. In this context raw data are single measurements like temperature or pressure readings. All further processing is based on the totality of data. This approach is able to yield the most accurate results, but it requires the sensors to be commensurate, i.e. that the different data can be processed in a common framework. If the data are in different regimes they have to be registered first, e.g. through coordinate transformations. Data-level fusion requires centralized data processing, since the totality of raw data has to be simultaneously available. A high communication bandwidth is necessary since all raw data have to be transferred. In feature-level fusion the raw data of each sensor are processed locally. A feature vector is generated from the corresponding observations. Features can, e.g., be volume fractions of materials, flow rates, or flow profiles, which are derived from multiple single point measurements. The different vectors are then fused to give a single feature vector. The necessary communication bandwidth is reduced compared to data-level fusion. However, the generation of the single feature vectors results in some data loss in general. Finally, in decision-level fusion, each sensor derives higher-level decisions from its own data and features. A decision could be whether there is a process malfunction or not. The individual decisions are finally fused by some sort of voting to give the final inference. The high required bandwidth in data-level fusion may be a severe disadvantage in large scale distributed target tracking applications,

but is not regarded as a major issue in process instrumentation. Sensors that share a common or similar state space or reference frame are usually installed in close vicinity. In distributed production environments the derived feature and decision information is passed on to the control room.

This chapter is intended to give an overview of applications of model-based data fusion in the context of industrial instrumentation and process monitoring. The diverse examples addressed are grouped according to a classification in: uniquely determined, overdetermined, underdetermined, or sequential data fusion (Tanner, 2003). Data fusion may already take place in instruments that are received as single sensor installations from an outside perspective (Ruhm, 2007). Examples are sensors that rely on additional measured quantities to compensate for unwanted cross-sensitivities. Internal temperature compensation of the primary measurand, e.g., is indispensable in many instruments. A next step is data fusion of multiple independent and non-redundant sensors to compensate for cross-sensitivities among the primary measurands that can be explicitly modelled. A typical application is the concentration measurement in ternary or multinary solutions. A characteristic feature of this class of sensor fusion problems is that the number of unknown parameters can be uniquely determined from the number of input quantities of the fusion process.

A concept more easily perceived as data fusion is the combination of identical parallel sensors to provide redundant information. This leads to a higher degree of security and reduces measurement uncertainty. The use of such redundant sensor arrays has a long tradition in industrial process instrumentation as sensor breakdowns and false decisions can have dramatic implications. Even single sensor failures may be able to cause malfunctions of large-scale facilities like power plants if security issues are not properly addressed in the system architecture. A slightly different approach than redundancy maximization is the use of identical sensors in a specific spatial configuration. By using appropriate models it is then possible to deduce quantities that cannot be measured with a single point sensor of the same measurement principle. Further benefits are increased accuracy of the estimates and powerful error compensation without additional sensors. This approach is convincing if very simple and cost-efficient elements can be used and will be illustrated by means of capacitive and magnetic sensors for angular position measurement. In these cases the number of measurement values exceeds the number of unknown parameters to be determined.

The third class of data fusion applications covers the converse case where the number of independent measurements from a homogeneous sensor array is actually smaller than the number of unknown parameters. This occurs when spatially varying material parameters are to be determined using industrial process tomography. The number of measurements obtained at the boundary of a problem domain is limited compared to the appropriate discretization of the domain. This leads to ill-posed inverse problems. The incorporation of additional prior knowledge through the process model is essential in order to obtain a meaningful solution of the problem. Here the concept of model-based measurement peaks in its relevance as a framework for multi-sensor data fusion. Solution strategies for tomographic problems are introduced in the corresponding section and the importance of the process model is discussed. Besides single-modality tomographic data fusion, multi-modality fusion is also addressed. For this case a sequential fusion process is proposed.

In subsequent sections, grouped according to uniqueness of the data fusion solution, several model formulations will be introduced. These model formulations range from static to dynamic, ideal to those including nuisance effects and noise, and explicit to implicit. Also different fusion algorithms including response surfaces, stochastic filters, and sequential fusion will be addressed within the respective applications.

2. Non-redundant measurement processes

2.1 Error compensation

Measurement processes and the superordinate fusion algorithms can be modelled in various ways. Depending on the actual situation and the aim of the measurement they may be formulated as static or dynamic systems. For certain applications a static model may be sufficient although virtually every sensor shows some kind of dynamic behaviour. For the following considerations we assume a vector $z^T = (z_1 \quad z_2 \quad ...)$ of two or more measurements as input to a nonlinear static fusion equation f.

$$x = f(z) \tag{1}$$

The output of the fusion process is the scalar variable x. This kind of data fusion can already be found in most of modern process instruments. In the simplest case a single input variable is directly related to the output of the fusion relation and defines the primary measurement equation. An illustrative example that can be found throughout the process industries is density measurement. A classical instrument for that purpose is the vibrating tube densimeter (Ihmels et al., 2000) (Laznickova & Huemer, 1998). The operating principle based on a spring-mass system is sketched in figure 1 using a U-shaped tube. The process fluid under test flows through a metal or glass tube that is decoupled from the surrounding through a base mass. In order to measure the fluid density the tube is excited by a force acting on the bend. The tube then vibrates at its resonant frequency, which is sensed by the pick-up mechanism.

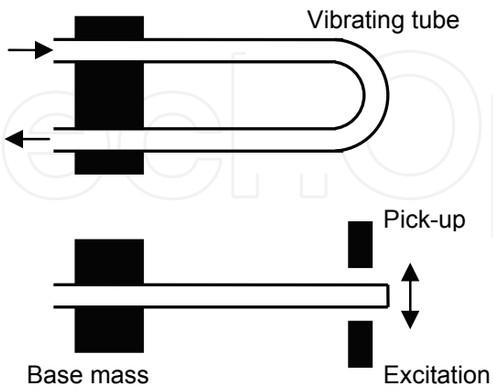

Fig. 1. Principle of the vibrating tube densimeter.

The resonant frequency depends on the mass m_T of the tube and the mass of the fluid m_F inside the tube. With the spring constant c the relation for the resonant frequency f_R and the period of oscillation τ_R can be obtained.

$$f_R = \frac{1}{\tau_R} = \frac{1}{2\pi}\sqrt{\frac{c}{m_T + m_F}} \tag{2}$$

As the volume of the tube is constant and known the measurement is proportional to the fluid density. Equation (2) can be reformulated to give the density ρ as a function of the period of oscillation, where *A* and *B* are constants.

$$\rho = A\tau^2 + B \tag{3}$$

In practice equation (3) is not sufficient to obtain accurate results over a wide operating range as there are several other factors influencing the period of oscillation. Temperature changes lead to changes in the tube volume and the spring constant. The same holds for changes of the fluid pressure p. To compensate for these effects a polynomial expansion can be applied to the constants in the measurement equation.

$$A = \sum_j a_j T^j + \sum_j b_j p^j \tag{4}$$

$$B = \sum_j c_j T^j + \sum_j d_j p^j \tag{5}$$

For increased accuracy also mixed terms can be included. Combining equations (3) – (5) we obtain the fusion equation to compensate for the nuisance effects of temperature and pressure on the density reading.

$$\rho = f(\tau, T, p) \tag{6}$$

As the accuracy requirements are increased even further influences need to be compensated for. Fluid viscosity, as an example, is known to have a small effect on the period of oscillation (Krasser & Senn, 2007).

2.2 Multidimensional parameter estimation

In the error compensation case several auxiliary measurands act on individual scalar output quantities in a unidirectional way. A more complex fusion process can be introduced if a vector of output quantities $x^T = (x_1 \quad x_2 \quad \ldots)$ is introduced in equation (1). Then the input parameters can interact with all of the outputs simultaneously. This allows for the use of more flexible and powerful fusion methods. Figure 2 shows flow charts of the scalar and multidimensional data fusion approaches. The data fusion process f_{12} can range from a matrix in the linear case to arbitrary response surface methods, e.g. based on polynomial expansions.

The concentration measurement of ternary and multinary solutions is a typical problem in this class of fusion procedures. The density measurement introduced in section 2.1 is often used for concentration measurement of binary solutions. However, if there are more than two components only the sum of contributions of the individual components can be measured. The measurement problem may be resolved by fusing suitable methods for binary concentration measurement. As a representative application the measurement of extract and alcohol concentration in beer production is presented (Vasarhelyi, 1977). Beer is

basically a ternary mixture of water, extract and alcohol. So density measurement alone is not sufficient. The same is true for sound velocity and refractive index measurements, which are also classical methods for density and concentration determination (Hauptmann et al., 2002). If the response curves of two measured quantities to extract and alcohol variations are linearly independent in a certain range the problem can be solved with data fusion. Then both quantities can be uniquely determined from the primary measurements. The procedure is sketched in figure 3.

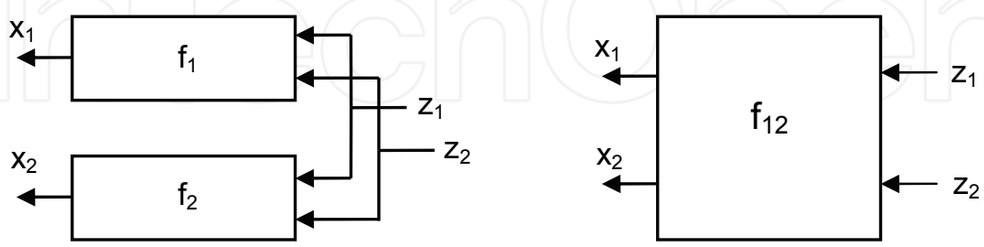

Fig. 2. Data fusion by means of unidirectional error compensation (left) and multi-dimensional parameter transformation (right).

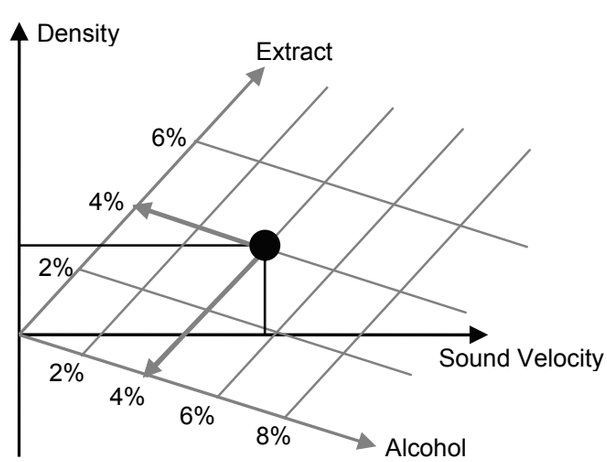

Fig. 3. Determination of extract and alcohol concentration in beer from density and sound velocity measurements.

The example qualitatively shows the extract and alcohol determination from density and sound velocity measurements. It can be seen that an extract change increases both sound velocity and density. On the contrary, a change of the alcohol concentration increases sound velocity and decreases density. This orthogonality allows for the unique determination of the target quantities. The inversion procedure corresponds to the transformation of a point in the Euclidean density/sound velocity space to a different, in general curvilinear, coordinate system.

3. Redundant measurement processes

3.1 Sensor fault detection and isolation

One of the most prominent applications of data fusion in industrial process instrumentation is sensor fault detection and isolation (FDI). It is of fundamental importance in all safety-

critical processes where the reliability of sensor data needs to be assured. Typical examples are nuclear power plants and other assets processing dangerous materials or handling very high power. In such cases false sensor readings may cause expensive and harmful damage. The central step in FDI is the generation of residuals. Residuals are functions of sensor outputs and must rise in case of a sensor fault (Betta & Pietrosanto, 2000) (Dorr et al., 1997) (Simani, 2000). Faults can then be detected by comparing the residuals with thresholds that are suitably defined with respect to the normal sensor operation. Finally the faulty sensors are isolated by analyzing the different residuals.

Physical and analytical redundancies are the two possible types of redundancy necessary for the calculation of residuals. Physical redundancy means the use of several sensors measuring the same physical quantity in parallel. Analytical redundancy is concerned with the application of analytical models in order to produce estimates of sensor signals from other sources of data. It requires the precise knowledge of the underlying process. Typically applied in this category are stochastic filters and observers like the Kalman filter. The application study in section 3.2 treats a sensor system using an extended Kalman filter with integrated FDI functionality.

Physical redundancy is more general as it does not rely on such information. However, it is more expensive to implement as multiple sensors for every quantity to be measured need to be employed. Residuals for a redundant set of sensors are computed by comparing each sensor signal with an estimate of the true value of the measured physical quantity ς. A straightforward linear measurement and fault model can be used to relate the true value to the measurement z_j of sensor j.

$$z_j = \varsigma + v_j + \delta_j \tag{7}$$

Each of the n sensor readings is corrupted with a random noise component v. The component δ_j is considered the contribution of an abnormal degradation or fault of sensor j. The individual sensor fault contributions are assumed independent. The estimate of the true value ς is obtained from a weighted sum of the sensor readings. Constant weights are used if the random contributions v are uncorrelated white Gaussian noise with the same variance. There are many different possibilities to derive and analyze the residual vector r for the redundant instruments. The proper choice depends on the assumed fault mechanisms and effects. A good choice for the introduced linear fault model is the difference of the individual sensor values and the calculated mean of the respective remaining measurements.

$$r_j = z_j - \frac{1}{n-1}\sum_{k=1,k\neq j}^{n} z_k \tag{8}$$

In the fault-free case the expectation of the residuals is zero and the standard deviation depends on the individual sensor standard deviations and the number of sensors.

$$\sigma(r_j) = \sqrt{\frac{n}{n-1}}\sigma(z_j) \tag{9}$$

In the case of a single instrument error the residual of this sensor has a mean equal to the fault amplitude, while the other residuals show a mean that is lower by a factor $1/(n-1)$. With this information suitable thresholds for the detection of occurring faults can be easily established.

Other possibilities for the detection of faults include the calculation of statistical, spectral, and temporal characteristics of the residuals and artificial intelligence methods. The use of fuzzy logic allows for a flexible integration of different aspects of failure modes with empirical knowledge, for which analytical models are difficult to define (Park & Lee, 1993). Input quantities of the system like differences of sensor values and other characteristics are fuzzified using linguistic variables. An example is shown in figure 4.

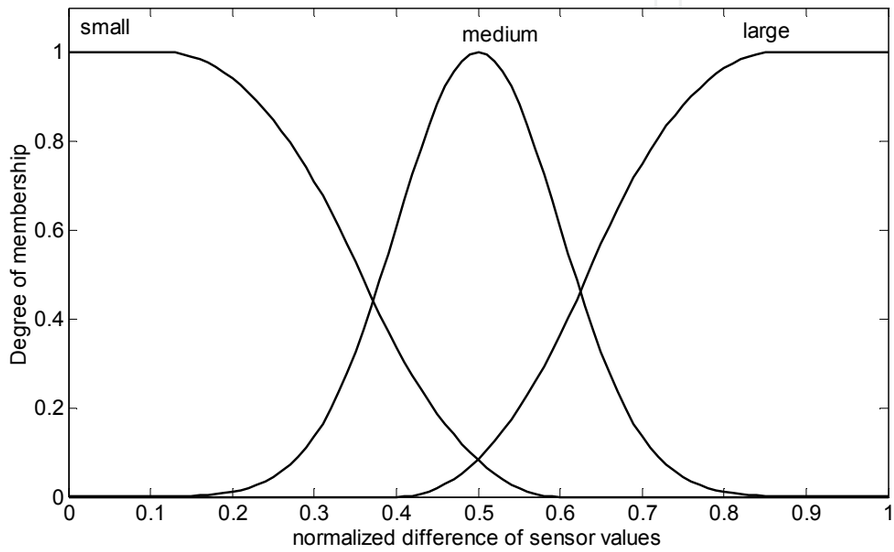

Fig. 4. Membership functions used for fuzzy-based fault detection and isolation.

The differences of sensor readings are normalized according to the standard uncertainties of the sensors. In the shown example three membership functions 'small', 'medium', and 'large', based on Gaussian and spline functions, are employed for the fuzzification (Steiner & Schweighofer, 2006). Further input variables can be elaborated from other observations related to error and fault occurrence. The actual fault model is contained in the rule base that is used for fuzzy inference. Rules are formulated as if-then relations.

$$\text{IF residual 1}=\textit{small}\ \text{AND residual 2}=\textit{small}\ \text{THEN operation}=\textit{normal} \tag{10}$$

The de-fuzzification stage of the Mamdani-type fuzzy system finally yields quantitative measures of the output fault parameters. Fuzzy systems have the advantage that they can be easily extended with more detailed application-specific process knowledge.

3.2 Integrated sensor arrays

With suitably designed sensor arrays and data fusion algorithms the tasks of error compensation and fault detection and isolation can be readily combined within a single instrument. Another potential feature is the highly accurate estimation of quantities of

interest through the combination of multiple low accuracy sensing elements. The achievable performance is illustrated in the following by means of an integrated smart capacitive sensor array for the determination of angular position and speed (Watzenig et al., 2003) (Watzenig & Steiner, 2004). The approach is based on the use of the extended Kalman filter (EKF), which is frequently used for data fusion in applications like target tracking. It offers a powerful framework also for industrial applications of data fusion. In contrast to the methods introduced in this chapter it is based on dynamical state space models and allows to monitor and exploit dynamical effects of the involved sensors and processes.

The capacitive angular position sensor consists of a rotor mounted coaxially between two stator plates. One stator plate corresponds to the transmitter. It is divided into 16 segments, the other stator contains the receiving electrode. The 16 segments of the transmitting electrode are electrically isolated from each other. The two stator plates are both bounded by an inner and an outer guarding ring connected to ground potential. The electrically conductive rotor is also grounded. It affects the coupling capacitances between the transmitter segments and the receiving electrode, dependent on its angular position. The used sinusoidal rotor shape yields a sinusoidal capacitance distribution. Segment driver and receiver electronics ensure that the received voltage signal amplitude is linearly dependent on the coupling capacitances. Figure 5 illustrates the axial view of a capacitive angular position sensor with approximately sinusoidal capacitance variation. In particular, a four-blade rotor in front of the transmitting electrode with 16 segments is shown. The receiving electrode is similar to the transmitting electrode, but without segmentation. Thus, the sensor array consists of 16 simple low resolution measurement channels which acquire data at different spatial orientations. The sensible combination of the channel data allows for the accurate estimation of angular position. The same principle can be applied to the measurement of other quantities like inclination angle, torque, liquid level, and flow. It can also be used with other physical sensing effects.

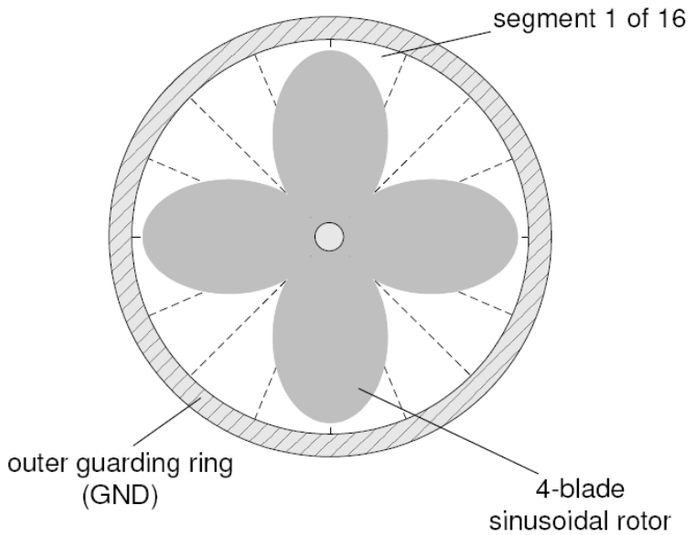

Fig. 5. Axial view of a capacitive angular position sensor. A four-blade rotor with a sinusoidal rotor shape is placed in front of the transmitting electrode, which is divided into 16 segments. The receiving electrode above the rotor is not shown.

The data fusion algorithm is based on the EKF. Therefore a discrete-time state space model of the sensor array is introduced. It is derived from a continuous second order system using a sampling interval T. The state vector x_k at time step k is composed of the angular position φ_k and the angular speed ω_k.

$$x_k = \begin{bmatrix} 1 & T \\ 0 & 1 \end{bmatrix} x_{k-1} + \begin{bmatrix} T \\ 1 \end{bmatrix} w_{k-1} \tag{11}$$

The measurement equation (12) relates the state vector to the vector z_k containing the 16 segment readings through the nonlinear measurement function h. Due to the special shape of the rotor the segment voltages are basically phase-shifted sinusoids as a function of the angular position. Both state and measurement equations are corrupted by process and measurement noise sequences w and v, respectively. They are assumed to be uncorrelated white Gaussian sequences with covariance matrices Q and R.

$$z_k = h(x_k) + v_k \tag{12}$$

The EKF recursively estimates the process states based on the current values of the states and the state error covariance matrix P_k. The algorithm can be grouped in a prediction step and a correction step. First the states and covariance are projected to the next time step based on the process model. The projected values are indicated by the superscript '-'. The correction uses the current measurement to update the projected states. The central equation is the calculation of the Kalman gain matrix K_k. It is based on a linearization of the measurement equation using the Jacobian H_k of h.

$$K_k = P_k^- H_k^T \left(H_k P_k^- H_k^T + R \right)^{-1} \tag{13}$$

The gain matrix is then used to update the state estimate using the current measurement.

$$\hat{x}_k = \hat{x}_k^- + K_k \left[z_k - h\left(\hat{x}_k^- \right) \right] \tag{14}$$

The term in brackets, which is the difference between actual measurement and estimated measurement, is called innovation sequence. It is a sensitive indicator of differences between a fault-free model and the current system. If the measurements and the model are in agreement, it has a mean of zero. Thereby Kalman filtering can also conveniently be used for fault detection and isolation using analytical redundancy. For the present application the innovation sequence s_k can be used to compensate for occurring segment offsets. The measurement equation (12) can be extended by offset voltages ξ for the individual segments.

$$z_k = h(x_k) + v_k + \xi_k \tag{15}$$

The offset values can be estimated without increasing the size of the Kalman filter equation systems by directly integrating the innovation sequence.

$$\xi_{k+1} = \xi_k + \tau \cdot s_k \tag{16}$$

The choice of the integration time constant τ determines the trade off between smoothness of the estimates and bandwidth of the offset compensation. The relation of the discrete-time EKF to the capacitive sensor system is illustrated in figure 6. The 16 measured segment voltages are used as inputs to the EKF. Based on the fusion of all signals the EKF is able to calculate accurate estimates of angular position and speed.

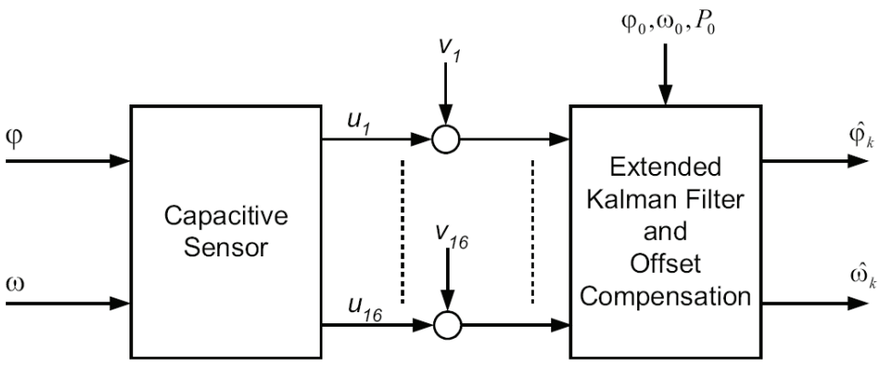

Fig. 6. Block diagram of the capacitive sensor with the extended Kalman Filtering with integrated offset estimation and compensation.

Figure 7 illustrates the performance of the EKF and the offset compensation approach. The first subfigure shows three of the measured sinusoidal voltages of adjacent segments. The second figure depicts the estimated segment offsets. There is a slight global offset at time step 0, which is compensated after about 10 samples. At time step 170 the voltage of segment 1, plotted bold, is stressed by an offset of 30% of the signal amplitude. The monitored innovation sequence is illustrated in subfigure 3. The sudden change in the amplitude of the sequence corresponding to segment 1 at time instant 170 (dashed vertical line) is obvious. The last chart shows the progression of the absolute angular position error.
A further approach to perform error compensation for the capacitive sensor array that is capable of handling additional errors like line faults, short circuits, driver failures, and electromagnetic disturbances, is to use several parallel Kalman filters and integrate the estimates in an additional data fusion step. Decentralized Kalman filtering also drastically reduces the computational requirements for the signal processing of the sensor array. In the present case the 16 measurement signals can be pairwise used as inputs to eight parallel EKFs. The inputs are wired in such a way that a single EKF processes signals that have a phase shift of 90°. The block diagram of the whole sensor system including the final fusion stage is sketched in figure 8.
All filters operate on the same process model, but use different measurement equations. Assuming equivalent error covariances for all filters, the decentralized fusion can be done by averaging the eight Kalman Filter state estimates. This assumption holds as long as no segment fault occurs.

$$\hat{\varphi}_k = \frac{1}{8}\sum_{j=1}^{8} \hat{\varphi}_k^{(j)} \tag{17}$$

By introducing fault detection with subsequent deactivation of certain filters with deficient state estimates the decentralized fusion can be applied for the general case. The fusion

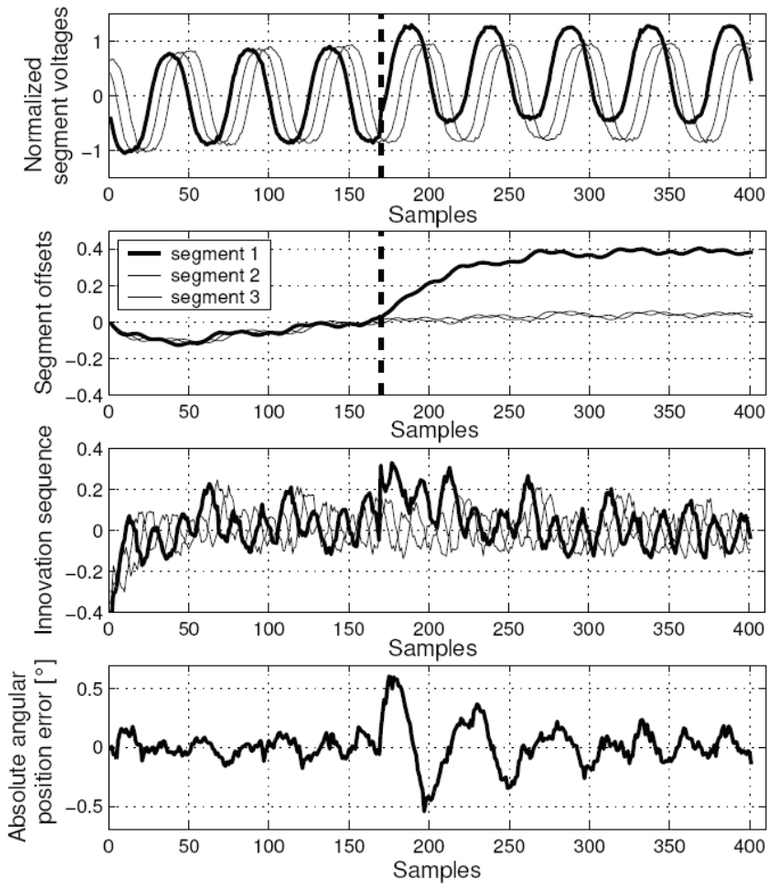

Fig. 7. Readings of the first three segments, segment offsets, monitored innovation sequence and curve of remaining angular position error. The signal of segment 1 is stressed by a DC offset at time step 170.

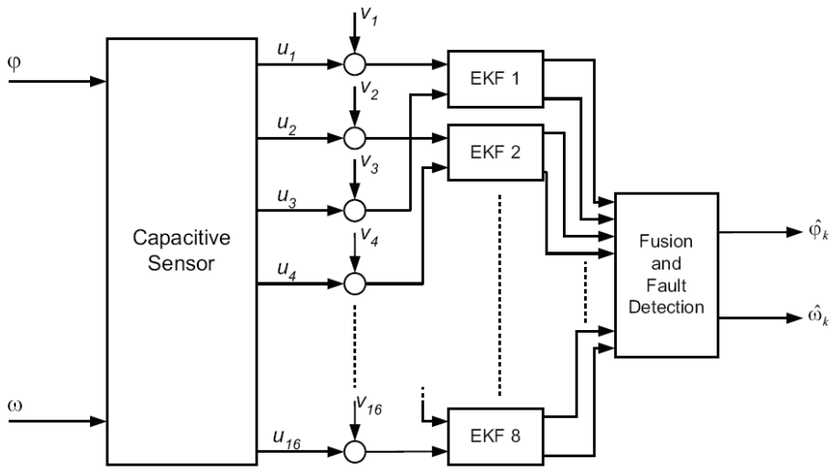

Fig. 8. Block diagram of the capacitive sensor with decentralized Kalman Filtering and subsequent data fusion with fault detection.

equation (11) does not consider the correlation of the single Kalman filter estimates due to the common process noise states. However, a comparison with the optimal fusion filter (Hashemipour et al., 1998) applied to the same problem shows only minor differences. The computational cost of the proposed averaging is very low compared to the optimal filter and numerical problems inherent in optimal fusion are avoided.
The availability of eight state estimates in parallel can be exploited for fault detection. The correlation between the different outputs and the final averaged estimate provides a confidence figure (an estimate for the variance) for each filter output.

$$V_k^{(j)} = \frac{1}{N}\sum_{j=1}^{N}\left(\hat{\varphi}_k^{(j)} - \hat{\varphi}_k\right)^2 \tag{18}$$

The last N measurements are used for the calculation of the mean square difference. In order to exclude a faulty filter some threshold level must be defined. This threshold level should be adaptive in a sense that only a segment that is significantly worse than the others is eliminated. A possible choice is the mean of the confidence figures with a tuning parameter α.

$$V_k^{\max} = \frac{\alpha}{8}\sum_{j=1}^{8} V_k^{(j)} \tag{19}$$

The performance of the decentralized filtering approach to data fusion with the capacitive sensor array is demonstrated with two failure modes; segment drift, and segment disturbance. In capacitive sensing a line break does not necessarily lead to a full breakdown of the segment signal, because the capacitive coupling over a break is still considerable. Since this coupling may depend on external influences such as temperature or vibrations, a noisy segment signal as shown in figure 9 may occur. The noise contamination of one signal instantaneously affects the position estimate of the corresponding filter. The confidence figure of this filter quickly rises above the threshold, so that the corrupted EKF is excluded from the calculation of the final estimate. It can be included again when the variance estimate is below the threshold again.
Another failure mode is demonstrated in figure 10. The offset for one segment continuously increases. This occurs in practical implementations when, e.g., water drops or dirt accumulate on a segment, because the high conductivity or permittivity of such a contamination lead to an amplification of the signal. Again, this error is quickly detected, long before even a very restrictive range checking algorithm would have the chance to detect this problem. Consequently the angular position estimate remains unaffected from the disturbance.

4. Ill-posed measurement processes

4.1 Industrial process tomography

In some measurement problems the available data is not sufficient to fully characterize the process at hand. This is often the case in distributed scenarios where spatially varying quantities that cannot be measured directly need to be resolved. For example, tomographic measurement techniques are able to provide two-dimensional or three-dimensional information about internal states of industrial processes. The knowledge of the internal

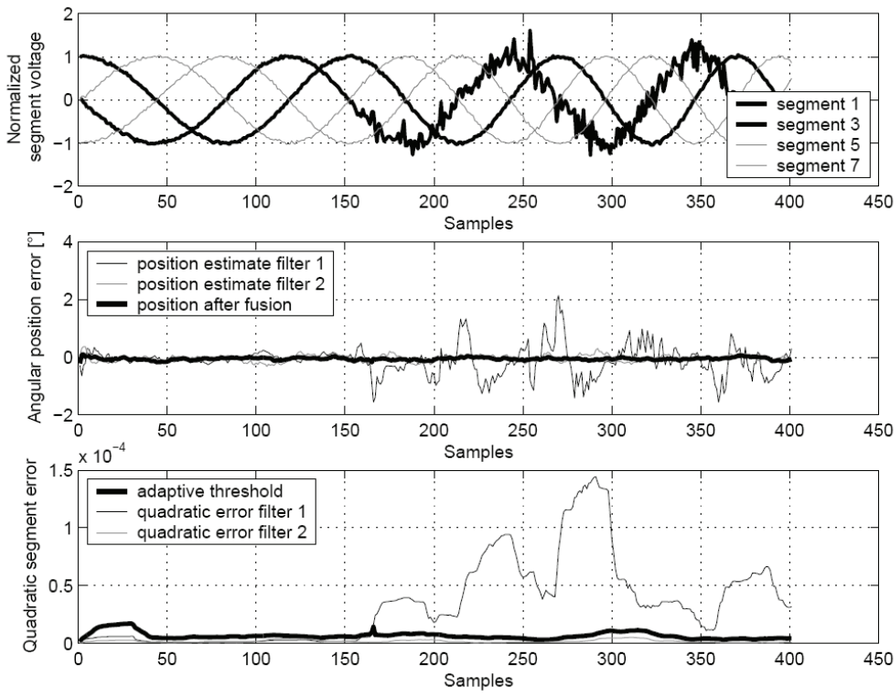

Fig. 9. Segment readings, output of selected filters, fused result, and adaptive threshold level in the case of a segment disturbance caused by a crack in the line.

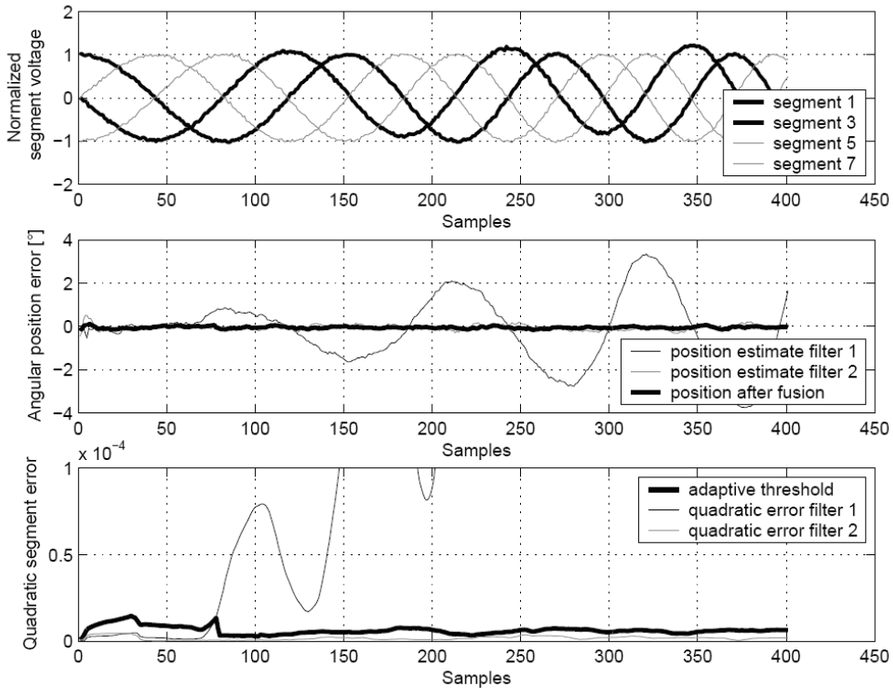

Fig. 10. Segment readings, output of selected filters, fused result and adaptive threshold level in presence of a segment offset drift.

behavior of such processes can be used for process design, prediction and process control in order to increase product quality and process efficiency. Depending on the application, different tomographic sensing modalities have been developed for industrial purposes, e.g. electrical capacitance tomography (ECT), electrical resistance tomography (ERT), ultrasonic reflection tomography (URT), positron emission tomography (PET) and X-Ray tomography (Scott & McCann, 2005) (Plaskowski et al., 1995). These techniques have in common that the spatially distributed parameters are reconstructed from a limited number of measurements. The sensors are usually distributed around the boundary of the problem domain. The fusion of this boundary data in order to obtain estimates of the spatial distributions of the quantities of interest is an ill-posed inverse problems. This implies that there is no unique solution to the problem. Ill-posed problems are very sensitive to noise and special measures need to be taken to obtain a stable meaningful solution (Kak & Slaney, 2001). This includes the choice of a suitable model of the measurement process and the incorporation of available prior knowledge through regularization. A multitude of reconstruction algorithms has been proposed, ranging from simple linear backprojection methods to model-based approaches based on nonlinear optimization methods and stochastic filtering methods like extended Kalman filters and particle filters.

Electrical capacitance tomography presents as a representative example. The objective in industrial ECT is to estimate the dielectric properties of heterogeneous mixtures or distinct transitions between occurring phases based on capacitance measurements between certain electrodes at the boundary of a closed container like a pipeline. Figure 11 illustrates the schematic of an ECT sensor based on the measurement of displacement currents (Wegleiter et al., 2005). The cross-section of a non-conducting pipe is used as measurement plane. 16 electrodes are evenly spaced around the circumference of the pipe. The setup is protected from electromagnetic interference by a grounded outer shield.

Every single electrode can be alternately used as a transmitter and a receiver. The front-end electronics of an electrode consists of a transmitting amplifier and an input stage comprising a current-to-voltage converter, a bandpass filter, and a high frequency peak rectifier. A single measurement frame consists of 16 projections, according to the 16 available transmitting electrodes. For one projection a specific electrode acts as transmitter while all the others sense the displacement current. A measurement frame consequently consists of 16 by 15 = 240 entries.

The reconstruction of the permittivity distribution within the pipe from the boundary measurements requires a mathematical model of the measurement process. This forward model establishes the functional mapping between the cross-sectional material distribution $\varepsilon_r(x, y)$ and the measured displacement currents q. Under the assumption of non-conducting materials, negligible magnetic fields, and wave propagation effects it can be modelled as an electrostatic field problem in the interior of the screen. This leads to a generalized Laplace equation for the electric potential v (Watzenig et al., 2007b).

$$\nabla \cdot (\varepsilon_r \nabla v) = 0 \tag{20}$$

Dirichlet boundary conditions $v = v_0$ at the transmitting electrode and $v = 0$ at the sensing electrodes are prescribed. The charges at the electrodes are proportional to the displacement currents occurring with time-harmonic excitation. The electrode charges are determined by integration of the electric displacement along the electrode boundaries. The forward model

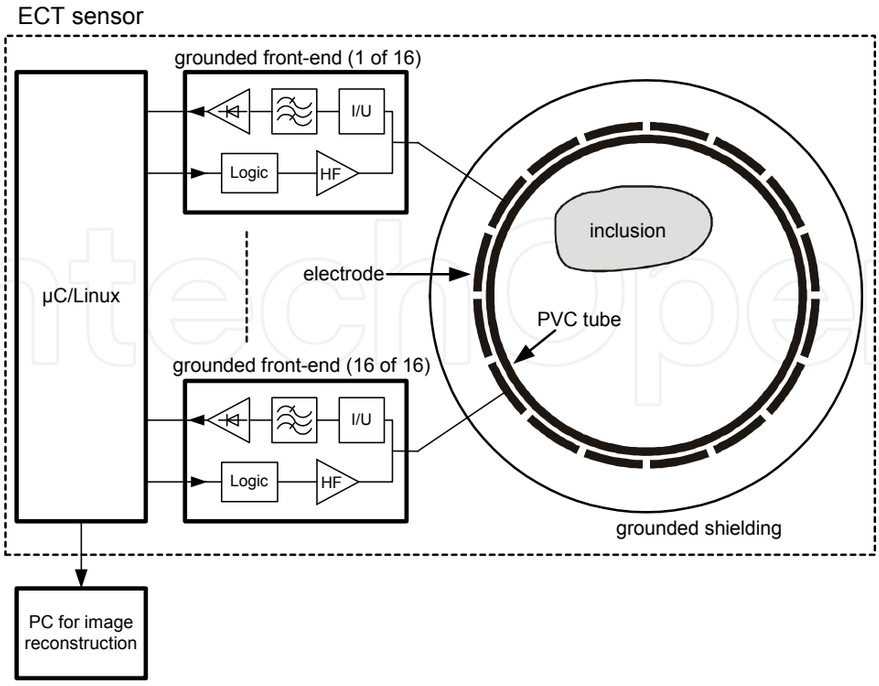

Fig. 11. Measurement configuration and schematic of a typical ECT sensor. The measurement electrodes are placed around the pipe containing the imaging domain. Every electrode features dedicated transmitting and receiving hardware. The acquired data is transferred to a PC where the signal processing is performed.

is numerically solved using the finite element method (FEM). The problem domain is thereby discretized into n triangular finite elements, where the permittivity is assumed constant within a single element. The discretization of equation (20) leads to a linear equation system for the vector v of the potentials of the finite element nodes.

$$K(\varepsilon_r)v = r \tag{21}$$

The stiffness matrix K reflects the geometry of the problem and the permittivities of the finite elements. Due to the sparsity of the stiffness matrix the equation system can be solved efficiently using specialized algorithms. However, in the context of industrial process tomography a compromise between the spatial resolution and accuracy of the finite element mesh and the computation time still has to be met. Figure 12 shows one quadrant of a typical finite element discretization. The domain is bounded by the outer screen. The interior contains the electrodes, the pipe and the imaging plane. The whole interior of the pipe is segmented into 316 elements, which is the number of unknown parameters to be reconstructed.

The unknown permittivity distribution can be estimated from the measured displacement currents by inverting the known measurement relation. A key issue associated with this inverse problem is its ill-posedness. This basically means that there is no unique solution and that it does not depend continuously on the data. The available reconstruction methods can be generally classified in non-iterative and iterative algorithms. Non-iterative methods assume a linear relationship between permittivities and displacement currents through the sensitivity matrix S.

$$q = S\varepsilon_r \tag{22}$$

This is an approximation since the actual relation is nonlinear. A linear reconstruction generates permittivity estimates from a pseudoinverse of the sensitivity matrix.

$$\hat{\varepsilon}_r = Dq \tag{23}$$

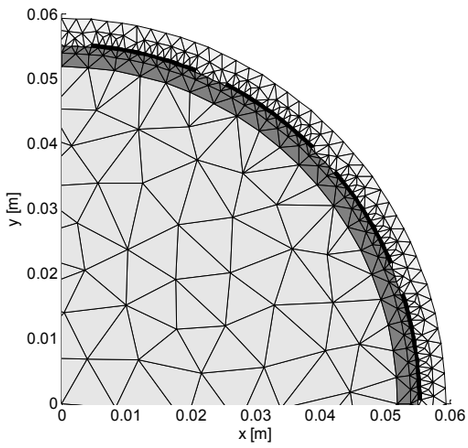

Fig. 12. Finite element discretization of one quadrant of the ECT problem domain. It consists of the electrodes (black), pipe (gray) and the imaging plane (light gray). The domain is bounded by the outer screen.

The pseudoinverse can be calculated in various ways. The simplest method is to use the transpose of the sensitivity matrix. More elaborate approaches like the offline iteration online reconstruction (OIOR) use an iterative precomputation.
More accurate results can be achieved with iterative methods that are based on the full nonlinear forward model.

$$q = f(\varepsilon_r) \tag{24}$$

In this case the inverse problem can be solved by minimizing a least squares cost functional. The minimization can be performed using the Gauss-Newton algorithm. A flow chart of the procedure starting from an initial guess for the permittivity distribution is sketched in figure 13. The minimization is terminated when the residual is below a predefined threshold.

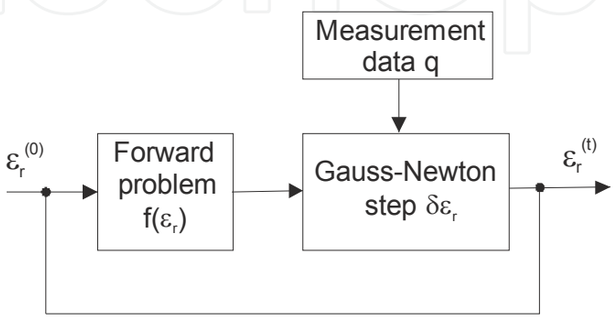

Fig. 13. Flow chart of the nonlinear least squares reconstruction for ECT.

$$C(\varepsilon_r) = \|q_m - f(\varepsilon_r)\|_2^2 + \alpha R(\varepsilon_r) \tag{25}$$

The first term on the right hand side of equation (25) is the sum of squared errors between measured displacement currents q_m and the simulated values. The minimization of this term alone would not yield sufficient results due to the ill-posedness of the inverse problem. Therefore a second term, the regularization term, has to be added in order to stabilize the solution. The relative weight of the two terms is controlled by the regularization parameter α. The assumptions that are placed in this term introduce prior knowledge about the assumed material distributions and can take various forms. A popular choice in the absence of specialized knowledge is generalized Tikhonov regularization.

$$R(\varepsilon_r) = \|L\varepsilon_r\|_2^2 \tag{26}$$

The regularization matrix L is a discrete approximation of the Laplace operator, leading to high values of R for jumps between neighboring finite elements. Consequently, this choice leads to a smoothing of the reconstructed permittivity distribution.
Figure 14 illustrates an ECT sensor with a predefined two-phase material composition of gravel and air (left). The reconstructed cross-sectional material distribution based on the described least squares reconstruction method with Tikhonov regularization is shown on the right. The relative permittivity values are coded in gray scale.

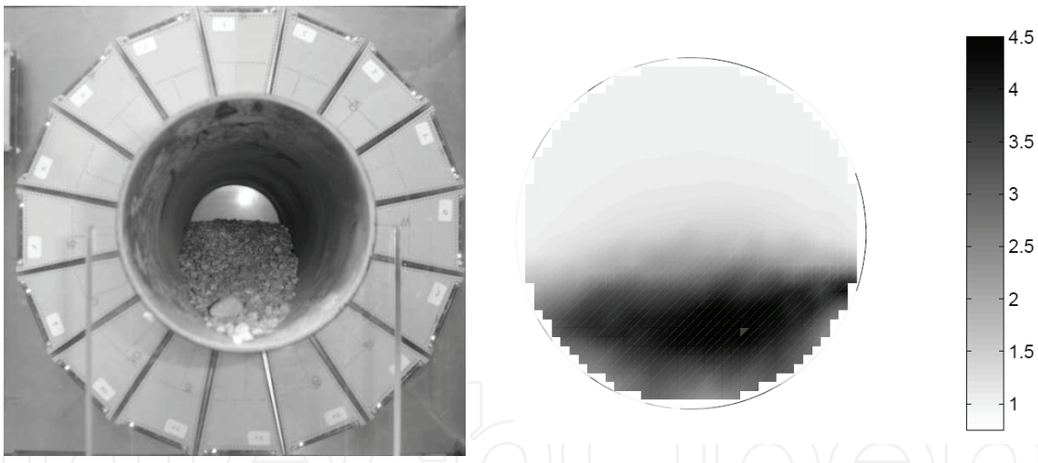

Fig. 14. ECT sensor partly filled with gravel (left) and the corresponding least squares reconstruction (right).

Depending on the industrial process at hand, models of the material distribution other than those described may replicate the situation more accurately. This allows to incorporate more detailed prior knowledge and helps to obtain accurate reconstruction results. Usually the materials involved in a process are known in advance. This sets constraints on the admissible parameter range (Steiner & Watzenig, 2008). When the distribution is piece-wise constant, like in discrete multi-phase flow, closed contour models would be appropriate. Boundaries between different materials are explicitly modelled, which introduces process-specific additional prior knowledge. Contour models can e.g. be based on polynomial splines, Fourier series expansions, and level set functions (Kortschak et al., 2007) (Watzenig

et al., 2007a). Closed Fourier contours in two dimensions can be obtained through parameterizations of the x and y coordinates with a period T=1.

$$x(t) = \frac{a_{x,0}}{2} + \frac{1}{2\pi}\sum_{j=1}^{N-1}\left[a_{x,j}\cos(2\pi js) + a_{b,j}\sin(2\pi js)\right] \tag{27}$$

The parameterization is similar for the other coordinate. The complexity of shapes that can be modelled can be increased by using more terms. The reconstruction can be performed by fitting the model parameters to the measurements, similar to the bulk model based on the finite element discretization.

Another sensing modality for industrial process tomography is ultrasound reflection tomography (URT). A common approach records reflections of transmitted ultrasonic waves at material boundaries. The measured travel times of reflected waves from many different directions can be used to reconstruct the locations and contours of material inhomogeneities. Also for URT there are different reconstruction approaches, from simple backprojection to model-based approaches utilizing specific contour models (Steiner et al., 2006). Results obtained with simple backprojection and a B-spline-based contour model and least squares minimization are illustrated in figure 15. The backprojection algorithm can be more generally applied to a wide range of problems. However, the results suffer from noise and blurring. If the process can be clearly characterized a proper model can lead to much better results, as demonstrated in the right subfigure.

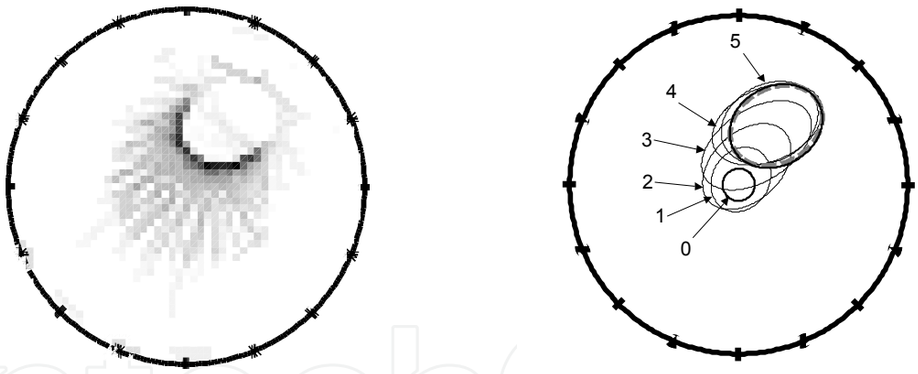

Fig. 15. URT reconstruction of a gas bubble in liquid. The left picture shows the results of a backprojection reconstruction. The right image shows the results obtained through using a contour model based on B-splines. The dashed ellipse shows the original bubble. The black curves show the evolution of the contour over the indicated iterations of the algorithm.

4.2 Tomographic sensor fusion

Multimodality tomography systems combine two or more different sensing modalities. The rationale is to increase the reconstruction accuracy by data fusion of complementary data. If sensibly combined, the multimodal data may contain more information about the state of the imaging domain than could be achieved with a single sensing modality alone. Multimodal sensors therefore offer the possibility to monitor complex processes that cannot be dealt with by single modalities. They can be fruitfully applied to three-phase flow, like

oil-gas-water flow occurring in oil production, where a single modality only gives good contrast for two of the involved materials. ECT and URT, e.g., are well suited for data fusion. The main motivation is that the electrical modalities are sensitive to the bulk properties of materials while ultrasound is sensitive to phase boundaries, yielding the desired complementarity. So URT can give accurate boundary information not available with electrical tomography and electrical tomography can give information about connected volumes not achievable with URT alone (Steiner, 2006).
The most widely used principle of dual modality data fusion in terms of the data flow is sequential coupling of the modalities, which is illustrated in figure 16. After individual acquisition of the raw data with the two sensor arrays the inversion of the first modality is independently performed. The result is then used as additional input for the reconstruction of the second modality. This can be seen as providing a priori knowledge about the process state for the second stage. Another option for the combination of two modalities is parallel processing of the totality of raw data. However, this raises serious issues of data association (Steiner, 2007).

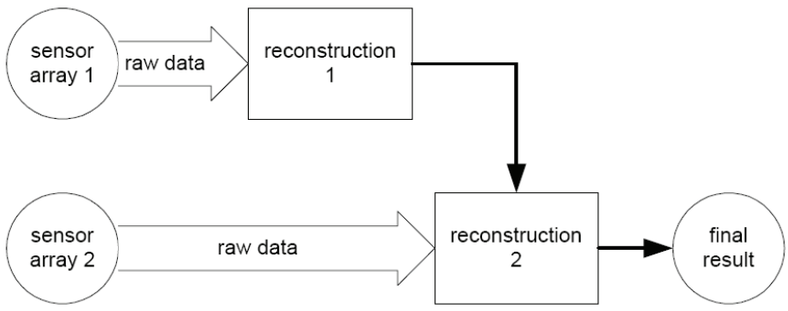

Fig. 16. Sensor fusion of two tomographic sensing modalities through sequential coupling of the raw data.

For the particular combination of sequential URT-ECT fusion the URT reconstruction can be used to deduce an outer approximation of the inclusion region containing the disperse phase of the material distribution, i.e. to uniquely assign parts of the imaging domain to the background region. If used in the subsequent ECT reconstruction, this information reduces the degrees of freedom of the inverse problem and thus the ill-posedness of the problem. Another approach is to use the incomplete information about object edges in the URT image to relax the smoothness assumption of ECT incorporated by the regularization term. This provides physically sound regularization as locations with a high probability of occurring material interfaces are allowed to show steeper permittivity gradients. A combination of these two sequential fusion approaches is compared to a single ECT reconstruction of two objects in figure 17. The left picture shows the ECT result, where the two objects cannot be resolved by the least squares reconstruction algorithm with smoothing Tikhonov regularization. ECT is least sensitive in the center of the imaging region, leading to a low spatial resolution. In contrast, URT offers highest sensitivity in the central region. The fusion reconstruction, due to the additional prior information from URT, distinguishes clearly between the two material inclusions.
An URT image as prior information is able to supply information about material boundaries. This can straightforwardly be included in contour-based reconstruction

algorithms for ECT. An example result is shown in figure 18. The capacitance data was reconstructed using a level set approach, where the contour is generated from equipotential curves of a two-dimensional function. A common regularization approach in this case is to penalize the arc length of the contour. The URT reconstruction can be added to the regularization term, forcing the level set contour towards the URT reconstruction while still allowing for deviations. The ECT reconstruction of two bubbles in figure 18 shows some blurring compared to the true object contours. The URT reconstruction, containing a sparse collection of points located just at the object boundaries, gives the extra information to allow for a close match of the true contours.

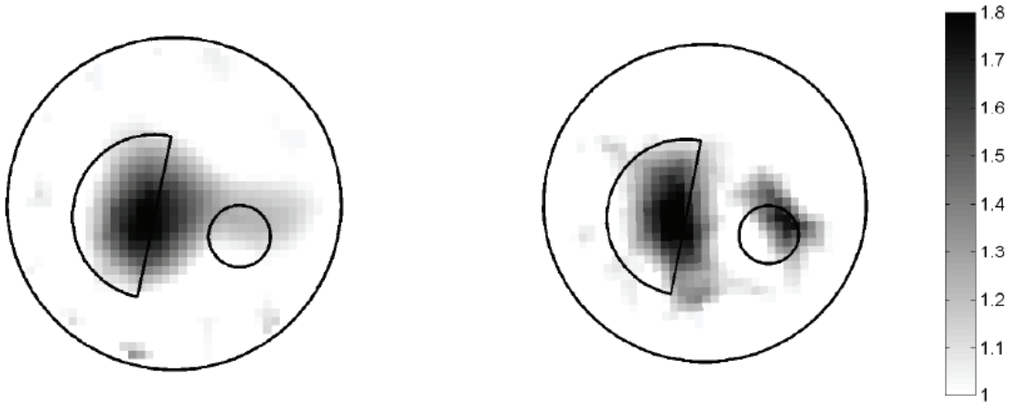

Fig. 17. Comparison of single ECT (left) and sequential URT-ECT fusion (right) reconstructions with a FEM-based spatial discretization of the imaging domain. The black curves show the true phase boundaries of the two material inclusions.

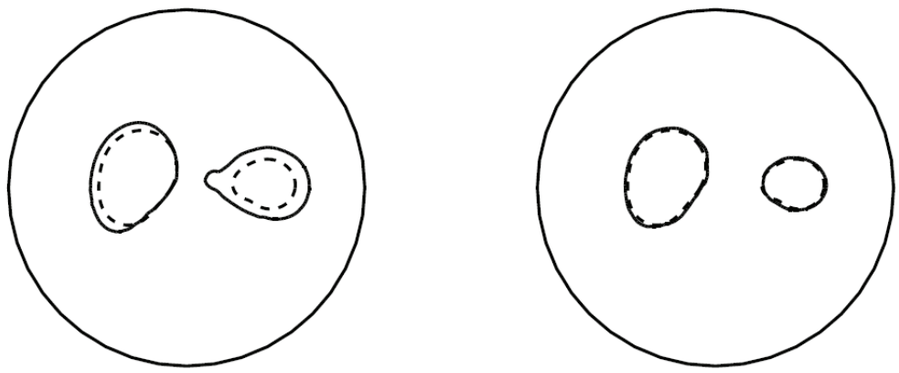

Fig. 18. Comparison of single ECT (left) and sequential URT-ECT fusion (right) reconstructions with a level set-based contour model. The dashed curves show the true phase boundaries of two material inclusions.

5. Conclusion

With increasing demands on the quality and efficiency of industrial processes as well as environmental and safety regulations, industrial process instrumentation is required to

acquire more accurate and comprehensive information. As the complexity of industrial processes increases, the same holds for the instrumentation. Data fusion techniques maximize the amount of useful information that can be extracted from raw sensor data.
This chapter gives an overview of model-based data fusion methods used in industrial process instrumentation with several typical application examples. They are intended to demonstrate the wide range of data fusion applications and are grouped in ascending complexity; from error compensation to multidimensional parameter estimation, sensor fault detection and isolation, integrated sensor arrays, industrial process tomography, and tomographic data fusion. It is expected that the consistent use of process models and data fusion methods will allow for an even more comprehensive and accurate characterization of industrial processes in the future.

6. Acknowledgement

This work was partially funded by the Austrian Science Fund (FWF) through the Translational Research Project L261-N04.

7. References

Betta, G. & Pietrosanto A. (2000). Instrument fault detection and isolation: State of the art and new research trends. *IEEE Transactions on Instrumentation and Measurement*, Vol. 49, No. 1, 100-107

Dorr R.; Kratz F.; Ragot J.; Loisy F. & Germain J.-L. (1997). Detection, isolation, and identification of sensor faults in nuclear power plants. *IEEE Transactions on Control Systems Technology*, Vol. 5, No. 1, 42-60

Hall D. L. & Llinas J. (1997). An introduction to multisensor data fusion. *Proceedings of the IEEE*, Vol. 85, No. 1, 6-23

Hall I. D.; McNab A. & Hayward G. (1999). Improved ultrasonic image generation through tomographic image fusion. *Ultrasonics*, Vol. 37,433-443

Hashemipour H. R.; Roy S. & Laub A. J. (1998). Decentralized structures for parallel Kalman filtering. *IEEE Transactions on Automatic Control*, Vol. 33, No. 1, 88-93

Hauptmann P.; Hoppe N. & Puettmer A. (2002). Application of ultrasonic sensors in the process industry. *Measurement Science & Technology*, Vol. 13, R73-R83

Ihmels E. C.; Aufderhaar C.; Rarey J. & Gmehling J. (2000) Computer-controlled vibrating tube densimeter for liquid density measurement in a wide temperature and pressure range. *Chemical Engineering Technology*, Vol. 23, No. 5, 409-412

Kak A. C. & Slaney M. (2001). *Principles of Computerized Tomographic Imaging*. Society of Industrial and Applied Mathematics, ISBN 139780898714944

Kortschak B.; Wegleiter H. & Brandstaetter B. (2007). Formulation of cost functionals for different measurement principles in nonlinear capacitance tomography. *Measurement Science and Technology*, Vol. 18, 71-78

Krasser E. & Senn H. (2007). Simultaneous measurements at U-tube density sensors in fundamental and harmonic oscillation. *Proceedings of the EUROCON 2007,* Warsaw, September 9-12, 551-555

Laznickova R. & Huemer H. (1998). Investigations on the limits of uncertainty of gas density measurements with vibrating tube densimeters. *Measurement Science & Technology,* Vol. 9, 719-733

Macii D.; Boni A.; De Cecco M. & Petri D. (2008). Multisensor data fusion. *IEEE Instrumentation & Measurement Magazine*, Vol. 11, No. 3, 24-33

Park S. & Lee C. S. G. (1993). Fusion-based sensor fault detection. *Proceedings of the International Symposium on Intelligent Control*, Chicago, August, 156-161

Plaskowski A.; Beck M. S.; Thorn R. & Dyakowski T. (1995). *Imaging Industrial Flows: Applications of Electrical Process Tomography*. Institute of Physics Publishing, ISBN 0750302968, Bristol, UK

Ruhm K. H. (2007) Sensor fusion and data fusion – Mapping and reconstruction. *Measurement*, Vol. 40, No. 2, 145-157

Scott D. M. & McCann H. (Ed.) (2005). *Process Imaging for Automatic Control*. Taylor & Francis, ISBN 0824759206

Simani S.; Fantuzzi C. & Beghelli S. (2000). Diagnosis techniques for sensor faults of industrial processes. *IEEE Transactions on Control Systems Technology*, Vol. 8, No.5, 848-855

Steiner G. (2006). Sequential fusion of ultrasound and electrical capacitance tomography. *International Journal of Information and System Sciences*, Vol. 2, No. 4, 484-497

Steiner G. & Schweighofer B. (2006). Parameter identification for a complex lead-acid battery model by combining fuzzy control and stochastic optimization. *Inverse Problems in Science and Engineering*, Vol. 14, No. 6, 665-685

Steiner G.; Podd F. J.W.; Brandner M. & Watzenig D. (2006) Iterative model-based image reconstruction for ultrasound process tomography. *Proceedings of the XVIII IMEKO World Congress*, Rio de Janeiro, September 17-22

Steiner G. (2007). Application and data fusion of different sensor modalities in tomographic imaging. *Elektrotechnik & Informationstechnik*, Vol. 124, No. 7/8, 232-239

Steiner G. & Watzenig D. (2008) Electrical capacitance tomography with physical bound constraints. *Proceedings of the SICE Annual Conference*, Tokyo, August 20-22, 1100-1105

Tanner R. & Loh N. K. (2003). A taxonomy of multi-sensor fusion. *Journal of Manufacturing Systems*, Vol. 11, No. 5, 314-325

Varshney P. K. (1997). Multisensor data fusion. *Electronics and Communication Engineering Journal*, Vol. 9, No. 6, 245-253

Vasarhelyi G. (1977). New possibilities of calculating alcohol, extract and original gravity of beer using refraction and density measurements. *Brauwissenschaft*, Vol. 30, No. 8, 239-244

Watzenig D.; Steiner G. & Zangl H. (2003). Capacitive sensor signal processing based on decentralized Kalman filtering. *Proceedings of the IEEE International Conference on Industrial Technology (ICIT)*, Maribor, December 10-12, 333-338

Watzenig D. & Steiner G. (2004). Offset compensation for capacitive angular position sensors by evaluating the Kalman filter innovation sequence. *Proceedings of the IEEE International Conference on Industrial Technology (ICIT)*, Hammamet, December 8-10

Watzenig D.; Brandner M. & Steiner G. (2007a). A particle filter approach for tomographic imaging based on different state-space representations. *Measurement Science and Technology*, Vol. 18, 30-40

Watzenig D.; Steiner G.; Fuchs A. & Brasseur G. (2007b). On-line estimation of process parameters in multi-phase flows from measured electrical capacitance data. Proceedings of the 13th International Sensor Conference, Nuernberg, May 22-24, 223-228.

Wegleiter H.; Fuchs A.; Holler G. & Kortschak B. (2005) Analysis of hardware concepts for electrical capacitance tomography applications. *Proceedings of the IEEE Conference on Sensors*, October 31 - November 3, Irvine, 688-691

Sensor and Data Fusion

Edited by Nada Milisavljevic

ISBN 978-3-902613-52-3
Hard cover, 436 pages
Publisher I-Tech Education and Publishing
Published online 01, February, 2009
Published in print edition February, 2009

Data fusion is a research area that is growing rapidly due to the fact that it provides means for combining pieces of information coming from different sources/sensors, resulting in ameliorated overall system performance (improved decision making, increased detection capabilities, diminished number of false alarms, improved reliability in various situations at hand) with respect to separate sensors/sources. Different data fusion methods have been developed in order to optimize the overall system output in a variety of applications for which data fusion might be useful: security (humanitarian, military), medical diagnosis, environmental monitoring, remote sensing, robotics, etc.

How to reference

In order to correctly reference this scholarly work, feel free to copy and paste the following:

Gerald Steiner (2009). Model-based Data Fusion in Industrial Process Instrumentation, Sensor and Data Fusion, Nada Milisavljevic (Ed.), ISBN: 978-3-902613-52-3, InTech, Available from: http://www.intechopen.com/books/sensor_and_data_fusion/model-based_data_fusion_in_industrial_process_instrumentation

INTECH
open science | open minds

InTech Europe
University Campus STeP Ri
Slavka Krautzeka 83/A
51000 Rijeka, Croatia
Phone: +385 (51) 770 447
Fax: +385 (51) 686 166
www.intechopen.com

InTech China
Unit 405, Office Block, Hotel Equatorial Shanghai
No.65, Yan An Road (West), Shanghai, 200040, China
中国上海市延安西路65号上海国际贵都大饭店办公楼405单元
Phone: +86-21-62489820
Fax: +86-21-62489821

IntechOpen